LBL-37716
UC-400

Lawrence Berkeley Laboratory
UNIVERSITY OF CALIFORNIA

EARTH SCIENCES DIVISION

Two-Phase Flow Experiments in Natural Rock Fractures from Yucca Mountain

P. Persoff and K. Pruess

September 1995

Prepared for the U.S. Department of Energy under Contract Number DE-AC03-76SF00098

DISCLAIMER

LBL - 37716
UC - 400

Two-Phase Flow Experiments in Natural Rock Fractures from Yucca Mountain

P. Persoff and K. Pruess

Earth Sciences Division
Lawrence Berkeley National Laboratory,
University of California
Berkeley, CA 94720

September 1995

This work was carried out for the Director, Office of Civilian Radioactive Waste Management, Yucca Mountain Site Characterization Project Office, under U.S. Department of Energy Contract No. DE-AC03-76SF00098.

Abstract

This is the second annual report on a series of laboratory measurements of two-phase flow in natural rock fractures from Yucca Mountain, Nevada. Two-phase (nitrogen gas and water) flow experiments have been conducted in a natural rock fracture (experiment G) and in two fractures formed by mating one half of a natural rock fracture to a transparent replica of the other half of the same fracture (experiments H and I).

Experiment G was conducted to confirm results obtained (Persoff et al. 1995) with a transparent replica of the same fracture (experiment E). The results of experiments E and G were generally similar. However, specific values of gas and liquid relative permeability were reached at greater capillary pressures (typically by a factor of 3) in the actual rock than in the replica. It is known that the contact angle of water on the replica material, θ, is greater than on the actual rock (where it is assumed to be zero). Therefore, at a particular degree of liquid saturation, the capillary pressure is greater in the actual rock than in the replica by a factor of $1/\cos\theta$. The observed difference in capillary pressures may be accounted for by the difference in wettability and less perfect matching of the replica fracture halves compared with the actual rock.

Because the substitution of a transparent replica for the actual rock introduces this systematic error in the capillary pressure, a series of experiments was planned in which a single sample would be examined four ways: as a replica, as the actual rock, and two rock-and-replica assemblies (Experiments H and I). In experiment H, a series of two-phase flow measurements was done in which the fracture was dried and then rewetted. Calculated liquid relative permeability showed hysteresis with respect to capillary pressure. This was also reflected in hysteresis in pore occupancy; that is, the regions which were last to desaturate were not necessarily the first to resaturate.

Introduction

The welded tuffs in the vadose zone of Yucca Mountain, Nevada, are being investigated as the potential site of a geologic repository for high-level nuclear wastes. The suitability of this site depends upon minimizing the possibility of aqueous transport of radionuclides from the wastes to the environment. The repository location has been chosen for its isolation by low-permeability rock from both the surface and the water table, in a desert area of low precipitation. The welded tuffs have very low (nanodarcy-microdarcy, or 10^{-21} - 10^{-18} m^2) permeability, offering protection from flowing groundwater.

The repository horizon, although of low permeability, is known to be fractured, suggesting the possibility of fast paths for contaminant transport.

As part of the repository evaluation, this study has been undertaken to characterize fractures from Yucca Mountain tuffs. Another purpose of this study is to gain insight into pore-level phenomena occurring during multi-phase flow in fractures generally. For this reason measurements were made not only in the actual fractures, but also in transparent replicas that reproduce the fracture void geometry. Use of transparent replicas allows observation of displacement phenomena and estimation of fracture saturation.

Samples

Experiments were done this year in an actual rock fracture (YM-3, experiment G), and in two fractures ("rock-and-replica") comprised of an actual rock fracture surface matched to a transparent replica of its mate. As reported last year (Persoff et al 1995), the source of these fractures were outcrop boulders from Fran Ridge and Yucca Mountain containing natural fractures, collected in November 1993 with the guidance and assistance of Alan Flint of the USGS. The fractures were pried open in the laboratory and photographed, and the two halves were arbitrarily designated "a" and "b." Transparent epoxy replicas of the fractures YM-1, -3, and -4 were made using molding and casting techniques described in Persoff and Pruess (1995). The fracture replicas were machined to 3-inch (75 mm) squares to fit the flow apparatus. The actual rock fracture YM-3 was also machined to fit the endcaps in preparation for further experiments.

Analysis of the results of two-phase flow experiments conducted in the YM-3 replica (experiment E, Persoff et al. 1995) and in the YM-3 rock (experiment G, reported below) showed that the difference in wettability between the rock and replica materials likely accounted for the observed differences in two phase flow behavior. Although use of transparent replicas allows valuable insight into displacement phenomena, the differences in wettability and possible inaccuracy in reproducing the fracture aperture require that capillary pressure measurements made in transparent replicas be adjusted if they are to be applied to actual rock fractures. To confirm this interpretation, a series of experiments was planned in which a single sample would be examined four ways: as a replica, as the actual rock, and two rock-and-replica assemblies. Although the 3-inch square area of the fracture YM-3 captured by the rock and replica samples were identical, the orientation of the fracture in the machined rock sample was not exactly the same as in the transparent replica. This made the existing replicas unsuitable for conducting rock-and-replica experiments for YM-3. Therefore a replica of YM-1 was prepared, and the actual rock YM-1 was machined to permit rock-and-replica experiments. These were used in experiment H and I.

Table 1. Natural fracture samples used in the experiments.

Sample	Location	Formation
YM-1	NE side of dune wash, west of Fran ridge	upper cliff of Topopah Springs welded
YM-3	NE side of dune wash, west of Fran ridge	Tiva Canyon columnar transition zone

Single- and Two-phase Flow measurements.

Flow measurements were done using the apparatus and techniques described elsewhere (Persoff and Pruess 1995; Persoff et al. 1994, 1995). Table 2 summarizes previously reported experiments (A-F) and the experiments reported here (G, H, and I). Essentially, the Hassler (1944) method for relative permeability measurements in porous cores was modified for fractures. This technique provides for capillary separation of the phases at inlet and outlet, and allows the capillary pressures to be measured and controlled as an independent experimental variable.

Fracture replicas were assembled to endcaps, and gas permeability was measured. Subsequently the fractures were flushed with CO_2 gas and then saturated with water, and liquid permeability measurements were made. Then gas and liquid were injected simultaneously for two-phase flow measurements. The approach taken was to establish a steady two-phase flow condition with a small gas saturation, and then reduce the liquid flow rate stepwise to obtain a series of steady states. After completing a series of measurements at increasingly dry conditions, the liquid flow rate was increased stepwise. The range of flow rates are summarized in Table 3 and in the Appendix. At each steady state, the outlet capillary pressure was made approximately equal to the inlet capillary pressure by adjusting the height of a water column on the liquid outlet line, adjusting a choke valve on the gas outlet line, or adjusting the gas injection pressure. In experiments H and I, videotape observations of the rock-and-replica fracture were used to detect changes in pore occupancy.

Experiment G (YM-3 actual rock)

In this experiment, the fracture was initially saturated. With constant liquid flow, gas flow was started. Initially, although gas injection pressure was constant, it was impossible to maintain constant gas flow. Gas flow (as indicated both by the inlet gas flowmeter (rotameter) and by gas bubbling from the exit line under water) would occasionally stop, and then the outlet gas and capillary pressures would decrease. By reducing the liquid flow rate, it was eventually possible to achieve steady flow conditions, and a series of 5 states (series 0) was explored with capillary pressures increasing from 0.2 to 0.5 psi (1.4 to 3.5 kPa). At the end of this series, we attempted to explore a series

Table 2. Two-phase flow experiments in rough-walled fractures.

Expt	Fracture	Hydro-dynamic aperture	Gas injection[a]	Data presentation
A	Stripa replica 1	8.5 μm	constant mass rate	Data in Persoff et al., 1991, and Persoff and Pruess 1995
B	Stripa replica 2	17.8 μm	constant mass rate	Videotape observations of liquid slug motion
C	Stripa natural rock	21.7 μm	constant mass rate	Data in Persoff and Pruess 1993, and Persoff and Pruess 1995
D	Dixie Valley replica	8.5 μm	constant pressure	Data in Persoff and Pruess 1993, and Persoff and Pruess 1995
E	Yucca Mountain replica YM-3	72 μm	constant pressure	Data in Persoff et al. 1995 (last year's report) and in Figs 1-4.
F	Yucca Mountain replica YM-4	130 μm	constant pressure	Data in Persoff et al. 1995 (last year's report).
G	Yucca Mountain rock YM-3	59 μm	constant pressure	Data in Figs. 1 - 4
H	Yucca Mountain rock-and-replica YM-1	133 μm	constant pressure	Data in Figs. 5, 6, and 20; fracture images in Figs. 7-19
I	Yucca Mountain rock-and-replica YM-1	141 μm	constant pressure	Two data points in Fig. 5, experiment still in progress.

[a] Liquid was injected at constant flow rate in all experiments

Table 3. Summary of data series run in experiments G and H.

Experiment	Series	Liquid Flow Rate Range (m^3/sec.)	Gas Flow Rate Range (m^3/sec.)	Saturation Direction
G	0	1.21E-10 - 1.04E-11	1.22E-8 - 1.56E-7	drying
G	1	8.33E-11	5.57e-8	wetting
H	0	8.33E-10 - 2.78E-12	3.83E-7 - 2.33E-7	drying
H	1	2.78E-12 - 2.22E-10	2.33E-7 - 3.83E-7	wetting

of steady states (series 1) in the wetting direction, by stepwise increasing the liquid flow rate. One such state was achieved, with capillary pressure 0.4 psi (2.8 kPa), but further increases in liquid flow rate resulted in intermittent gas flow as had been experienced at the start of the experiment. Thus there appeared to be a liquid flow rate above which constant gas flow could not be maintained (at least with pressure drop less than 0.2 psi [1.4 kPa]). As the liquid flow rate was reduced, and capillary pressure and gas saturation were increased, such intermittent blockage disappeared. Results of this experiment are summarized in the Appendix and appear in Figures 1 through 4.

Experiment H (YM-1 rock-and-replica)

In this experiment side "a" of the fracture was the rock, and side "b" was the replica. The fracture was initially saturated with water. With constant liquid flow, gas flow was started, and liquid flow was reduced as necessary to achieve a steady flow condition with steady pore occupancy. Then the liquid flow rate was decreased stepwise to reach a series of steady states at increasing capillary pressure. When the fracture was nearly dry, liquid flow rate was increased to reach a series of steady states in the wetting direction until steady gas flow could no longer be maintained. Video tapes and still images were analyzed to determine the changes in liquid saturation during the series of steady states. Results of this experiment are summarized in the Appendix and appear in Figures 5, 6, and 20. Images from this experiment are shown in Figures 7 through 19 and 21.

Experiment I (YM-1 rock-and-replica)

This experiment is conducted in the same manner as Experiment H, except that the rock and replica fracture halves have been reversed. At the time of this report, only the first two states have been recorded; these data are shown as additional points in Figure 5.

Permeability calculation. Fracture permeability is calculated from inlet and outlet pressures and flow rates, using modifications of the formulas for porous media (Persoff and Pruess 1995). In effect, one calculates the permeability k of the sample as if it were a porous medium of thickness h. The quantity h can also be thought of as the distance between uniformly spaced parallel fractures. For any set of pressure and flow rate data, the product hk is independent of the sample thickness and represents the permeability-thickness of the fracture. The calculated hydrodynamic apertures are shown in Table 2.

The permeability of a porous medium to gas is calculated by (Scheidegger, 1974)

$$k_g = \frac{2q_o \mu L p_o}{p_i^2 - p_o^2} \qquad ...(1)$$

where k is permeability, q is the darcy flow velocity or volumetric flux [L/t], μ is the viscosity, L is the length from inlet to outlet, subscripts i and o represent inlet and outlet conditions, respectively, and subscript g refers to gas. If flow is not through a porous medium but through a series of parallel fractures with spacing h, then both sides of equation (3) can be multiplied by h to give

$$hk_g = \frac{2hq_o \mu L p_o}{p_i^2 - p_o^2} \qquad ...(2)$$

Without knowledge of the fracture aperture, the value of q_o is not known, but the value of hq_o is known from continuity:

$$hq_o = \frac{Q_o}{w} \qquad ...(3)$$

where Q is the volumetric flow rate [L^3/t] and w is the length of the fracture edge at inlet and outlet. Similarly, k_L cannot be measured, but hk_L can be:

$$hk_L = \frac{hq\mu L}{p_i - p_o} \qquad (4)$$

where $hq = \frac{Q}{w}$; for incompressible fluids Q and q do not vary from inlet to outlet.

The effective hydrodynamic aperture of the fracture can be estimated from the data using the cubic law: the permeability of a parallel plate aperture of thickness b is $b^2/12$ (Witherspoon et al., 1980). If a series of plane parallel fractures with aperture b are separated by distance h, then the average permeability of the fractured medium is $(b^2/12)(b/h)$. Then

$$b = \sqrt[3]{12kh} \qquad ...(5)$$

Relative permeabilities were calculated as ratios of the measured effective kh for gas and liquid to the kh measured for single-phase liquid flow. Because in Experiment G the injected gas was dry, some evaporation of water occurred during flow through the fractures. For permeability

calculations, we assumed that gas was equilibrated with water in the inlet endcaps (i.e., entered the fracture at 100% relative humidity). The liquid flow rate was decreased and the gas flow rate was increased to account for the evaporated water. The effect of this correction on the calculated permeabilities is small. In Experiments H and I, injected gas was pre-humidified by bubbling through a water column. We assume that no evaporation occurred in the fracture; thus the flow rates are not corrected for evaporation. Again, calculated permeabilities are not sensitive to this assumption.

Results and Discussion

All primary measured data are summarized in Appendix A. From these data, relative permeabilities were calculated as described above.

Comparison of actual rock and replica. Figures 1, 2, and 3 show relative permeability in Experiment G plotted against capillary pressure, log capillary pressure, and gas:liquid flow rate ratio, respectively. Also shown are data from Experiment E (Persoff et al. 1995). Experiments E and G are intended as cross-comparison between the actual rock (G) the replica (E). The hydrodynamic aperture calculated from gas permeability measurements was 59 μm for the rock and 72 μm for the replica. The greater aperture for the replica probably results from inaccuracy in the replica surfaces leading to imperfect mating of the surfaces. In Figure 1, the sets of curves for the two experiments are generally parallel but the liquid relative permeability curves are offset by about 0.2 psi (1.4 kPa), and the gas permeability curves are offset by about 0.2 psi (1.4 kPa) plus a reduction in gas permeability by about 1 order of magnitude.

These differences are in accord with the difference in wettability of the fracture surface. Both surfaces are wet by water relative to air, but the contact angle is assumed zero for the rock, and has been measured at 70° for the epoxy replica by the captive-drop method (J.T. Geller, personal communication). From the Young-Laplace law, the capillary pressure needed to achieve any given degree of gas saturation in the fracture is greater in the rock than in the replica by the ratio ($\cos 0 / \cos\theta$). This implies that the curves should be parallel in Figure 2. The curves are not parallel (they are closer to parallel in Figure 1), but the offset factor, 2.9, is correct in magnitude and direction To a first approximation, therefore, the difference between the two experiments is accounted for by the difference in surface wettability. The measured hydraulic aperture of G is smaller than E (Table 2), indicating better mating of the surfaces.

In Figure 3 relative permeabilities measured in Experiment E and G are plotted as functions of gas:liquid flow rate ratio. These data show that

the fracture replica favors gas flow compared to the actual rock fracture, which is also in accord with the difference in surface wettability. In Figure 4, the relative permeabilities to gas and liquid are plotted against each other. These results show that the sum of the relative permeabilities is much less than 1, and again shows that the fracture replica favors gas flow compared to the actual rock fracture.

Hysteresis and Pore occupancy in a rock-and-replica fracture.

Figures 5 and 6 show relative permeability in Experiment H plotted against capillary pressure and gas:liquid flow rate ratio, respectively. The gas relative permeabilities measured in this experiment are anomalously high, possibly because of mismatched surfaces. In all other fractures tested, gas relative permeability at low capillary pressures has been much less than 1, and so has the sum of gas and liquid relative permeabilities. The two points measured thus far for Experiment I also agree with that trend. The gas relative permeability data for experiment H are thus difficult to account for. Since the gas flow is measured at the exit of the fracture by collecting gas in a graduated cylinder over water, there is no possibility of a gas leak causing larger flows of gas to be measured than actually flowed through the fracture.

The numbers assigned to points in Figure 5 represent the sequential order of the points in Experiment H (some numbers have not been assigned and are intentionally left out; the two points measured for Experiment I are also included for comparison). These data show hysteresis in both the gas and liquid relative permeabilities. Liquid permeability decreases with increasing capillary pressure, but the effect of capillary pressure on gas permeability is slight, and possibly lost in experimental error. On the rewetting cycle, liquid permeability was greater than in the drying cycle, and the gas permeability data show the reverse, suggesting that the increase in liquid permeability occurred at the expense of gas permeability.

Examination of images of the fracture during the steady states showed the changes in phase occupancy during the wetting and drying cycle. In this experiment, the water was dyed for visibility and the fracture was horizontal, with the replica on top. A video camera looked down into the fracture, which was illuminated obliquely from above. The colors seen in the images are by reflected, and not transmitted light. They therefore cannot be used to infer apertures, only the presence or absence of water which appears darker than the dry fracture. Images (selected to representing the most obvious changes in saturation) are shown in Figures 7 through 13. In these figures, the direction of flow is from left to right. The two vertical gray bars that appear in each picture are parts of the inlet and outlet endcap assemblies. Outside of these gray bars, the images are reflections of fracture, and can be ignored. These reflections are internal reflections in the Lucite blocks that compress the fracture. The red line at the top of the images is a flow

boundary; the opposite boundary is a gray line at the bottom edge of the image.

Figures 7 through 10 show the fracture is successive stages of increasing dryness as the capillary pressure was increased from 0.083 to 0.543 psi (570 to 3740 Pa). Figures 11 through 13 show the fracture is successive stages of increasing wetness as the capillary pressure was decreased from 0.642 psi back to 0.035 psi (4400 to 240 Pa). In these images three shades of blue can be distinguished: dark blue, as above the date in Fig. 7; medium blue as in the central portion of Fig. 8 and scattered throughout Fig. 9, and light violet, such as below the date in Fig. 9 and covering most of the fracture in Fig. 10. The dark blue is liquid filling the entire fracture aperture. During periods of changes in phase occupancy, this color showed such phenomena as bubble snap-off.

Identification of the medium blue and light violet is less certain. During the first part of the experiment, red dyed water was injected to the fracture, and the dye was changed to blue before these images were taken. As a result the rock has been dyed light violet. This permits two interpretations of the medium blue and violet areas: (i) the light violet represents areas where there is no water in the fracture and the matrix is unsaturated, and the medium blue represents areas where there is no water in the fracture and the matrix is saturated; or (ii) the light violet represents areas where there is no water in the fracture and the matrix is either saturated or unsaturated, and the medium blue represents areas where the matrix is saturated and there is a film of water on one of the fracture surfaces.

Changes in the dark blue areas in Figures 7 to 10 and 11 to 13 reveal how the fracture desaturated as the liquid flow rate was decreased, and capillary pressure increased, and then resaturated as the liquid flow rate was increased, and capillary pressure decreased. A digital imaging processing program, Adobe Photoshop, was used to display the differences between successive pairs of these digitized images. Because the water is blue, the intensity of blue light changes little when water is present, so changes in red light intensity were used to highlight changes in liquid saturation. The Photoshop "difference" routine does not distinguish between increase and decrease, but the direction of change can be seen by referring to the original images. Difference images, again selected to show the greatest changes in saturation, are shown in Figures 14 through 19. In these images unchanging areas show up as random dots due to noise in the images, while regions of saturation change appear as black areas, generally on the margins of the liquid-filled area of the fracture.

An attempt to establish a series of steady states starting with a dry fracture and matrix and injecting water (dyed red) was not successful, because the liquid pressure taps lost liquid continuity with the fracture. However, during this

effort data were collected during a period in which temperature, gas injection pressure, and liquid flow rate all remained steady, but the gas outlet pressure and outlet capillary pressures cycled regularly. The videotape of this period showed that the fracture saturation changed cyclically as well. The capillary pressure data for this period is shown in Figure 20. In this figure, the horizontal bars represent periods of time when the saturation was increasing (wetting) or decreasing (drying) or stable. Images of the fracture taken at four successive maxima and minima are shown in Figure 21. In these images, areas of the fracture that were never wet appear white, while light and dark red represent areas in which the fracture is filled by gas and liquid, respectively. Higher capillary pressure is clearly associated with reduction in liquid saturation (areas of desaturation are indicated by arrows in Figure 21) but the cause for this behavior is not clear. It may be a result of interaction between the fracture and the permeable rock side of the fracture.

Summary

Two-phase (nitrogen gas and water) flow experiments have been conducted in a natural rock fracture (YM-3, experiment G) and in two fractures formed by mating one half of a natural rock fracture to a transparent replica of the other half of the same fracture (YM-1, experiments H and I).

Experiment G was conducted to confirm results obtained previously with a transparent replica of the same fracture (experiment E). The results of experiments E and G were generally similar. However, specific values of gas and liquid relative permeability, which are assumed to represent particular values of saturation, were reached at greater capillary pressures (typically by a factor of 3) in the actual rock than in the replica. It is known that the contact angle of water on the replica material, θ, is greater than on the actual rock (where it is assumed to be zero). Therefore, at a particular degree of liquid saturation, the capillary pressure is greater in the actual rock than in the replica by a factor of $1/\cos\theta$. To a first approximation, this difference in wettability accounts for the observed difference in capillary pressures.

Because the substitution of a transparent replica for the actual rock introduces a systematic error in the capillary pressure, a series of experiments was planned in which a single sample would be examined four ways: as a replica, as the actual rock, and two rock-and-replica assemblies (Experiments H and I). In experiment H, a series of two-phase flow measurements was done in which the fracture was dried and then rewetted. Calculated liquid relative permeability showed hysteresis with respect to capillary pressure. This was also reflected in hysteresis in pore occupancy; that is, the regions which were last to desaturate were not necessarily the first to resaturate.

Acknowledgment

This work was carried out for the Director, Office of Civilian Radioactive Waste Management, Yucca Mountain Site Characterization Project Office, under U.S. Department of Energy Contract No. DE-AC03-76SF00098. We thank Alan Flint of the USGS for assistance in obtaining the fracture samples, Bing Tsai and Sanjay Gangadhara for assistance in carrying out the experiments, and our colleagues Lea Cox and Yvonne Tsang for reviewing the manuscript.

References

Hassler, G.L., Method and Apparatus for Permeability Measurements, U.S. Patent 2,345,935, 1944.

Persoff, P. and K. Pruess Two-Phase Flow Visualization and Relative Permeability Measurement in Natural Rough-Walled Rock Fractures, *Water Resources Research* 31 (5) 1175-1186 (1995) (Lawrence Berkeley Laboratory report LBL-35279)

Persoff, P., K. Pruess, and L. Myer, Method and Apparatus for Determining Two-Phase Flow in Rock Fracture, U.S. Patent 5,311,766, May 17, 1994.

Persoff, P. and K. Pruess, Flow Visualization and Relative Permeability Measurements in Rough-Walled Rock Fractures, High Level Radioactive Waste Management : Proceedings of the Fourth International Conference, Las Vegas NV, April 26-28, 1993, vol. 2, 2033-2041, American Society of Civil Engineers, New York, 1993 (LBL-33447).

Persoff, P., K. Pruess, and L. Myer, Two-Phase Flow Visualization and Relative Permeability Measurements in Transparent Replicas of Rough-Walled Rock Fractures, Proceedings, Sixteenth Workshop on Geothermal Reservoir Engineering, Stanford Univ., Stanford, CA., Jan. 23-25, 1991.

Persoff, P., K. Pruess, and L.P. Petersen, Progress on Flow Visualization and Relative Permeability Measurement in Transparent Replicas of Natural Fractures from Yucca Mountain (LBL-36614), January 1995.

Pruess, K., and Y.W. Tsang, On Two-Phase Relative Permeability and Capillary Pressure of Rough-Walled Rock Fractures, *Water Resources Research, 26* (9), 1915-1926, 1990.

Scheidegger, A.E., *The Physics of Flow Through Porous Media,* 3rd ed., University of Toronto Press, Toronto, 102, 1974.

Witherspoon, P.A., J.S.W. Wang, K. Iwai, J.E. Gale, Validity of Cubic Law for Fluid Flow in a Deformable Rock Fracture, *Water Resources Research, 16* (6), 1016-1024, 1990.

Figure Captions

Figure 1. Relative permeability (log scale) plotted against capillary pressure (linear scale), experiments E and G, fracture YM-3.

Figure 2. Relative permeability (log scale) plotted against log capillary pressure (log scale), experiments E and G, fracture YM-3.

Figure 3. Relative permeability plotted against gas:liquid mass flow ratio (log scales) , experiments E and G, fracture YM-3.

Figure 4. Gas and liquid relative permeabilities plotted against each other (log scales), experiments E and G, fracture YM-3.

Figure 5. Relative permeability (log scale) plotted against capillary pressure (linear scale), experiments H and I, rock-and-replica fracture YM-1.

Figure 6. Relative permeability plotted against gas:liquid mass flow ratio (log scales), experiments H and I, rock-and-replica fracture YM-1.

Figure 7. Image of fracture replica filled with dye, rock-and-replica YM-1, point 7 in Figure 5 (drying curve).

Figure 8. Image of fracture replica filled with dye, rock-and-replica YM-1, point 9 in Figure 5 (drying curve).

Figure 9. Image of fracture replica filled with dye, rock-and-replica YM-1, point 10 in Figure 5 (drying curve).

Figure 10. Image of fracture replica filled with dye, rock-and-replica YM-1, point 14 in Figure 5 (drying curve).

Figure 11. Image of fracture replica filled with dye, rock-and-replica YM-1, point 18 in Figure 5 (wetting curve).

Figure 12. Image of fracture replica filled with dye, rock-and-replica YM-1, point 20 in Figure 5 (wetting curve). .

Figure 13. Image of fracture replica filled with dye, rock-and-replica YM-1, point 23 in Figure 5 (wetting curve).

Figure 14. Image difference representing areas of desaturation between points 8 and 9 in Figure 5.

Figure 15. Image difference representing areas of desaturation between points 9 and 10 in Figure 5 .

Figure 16. Image difference representing areas of desaturation between points 10 and 14 in Figure 5.

Figure 17. Image difference representing areas of resaturation between points 17 and 18 in Figure 5..

Figure 18. Image difference representing areas of resaturation between points 19 and 20 in Figure 5

Figure 19. Image difference representing areas of resaturation between points 20 and 21 in Figure 5.

Figure 20. Changes in capillary pressure during steady inlet boundary conditions. Clock times are noted at two successive maxima and minima of inlet capillary pressure.

Figure 21. Images of fracture at times noted in Figure 20.

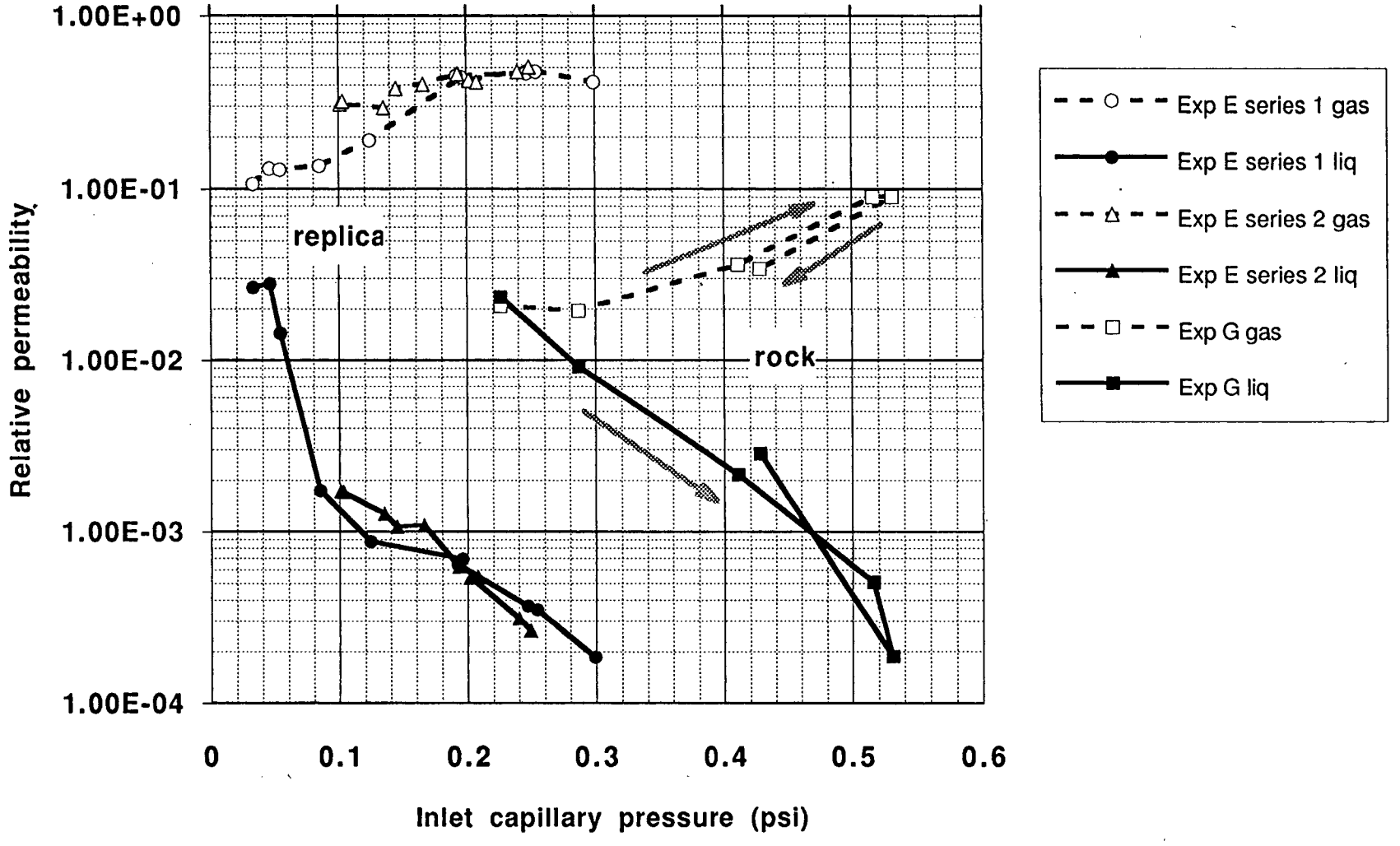
1.00E+00
1.00E-01
1.00E-02
1.00E-03
1.00E-04
Relative permeability
replica
rock
0
0.1
0.2
0.3
0.4
0.5
0.6
Inlet capillary pressure (psi)
Exp E series 1 gas
Exp E series 1 liq
Exp E series 2 gas
Exp E series 2 liq
Exp G gas
Exp G liq

Figure 1.

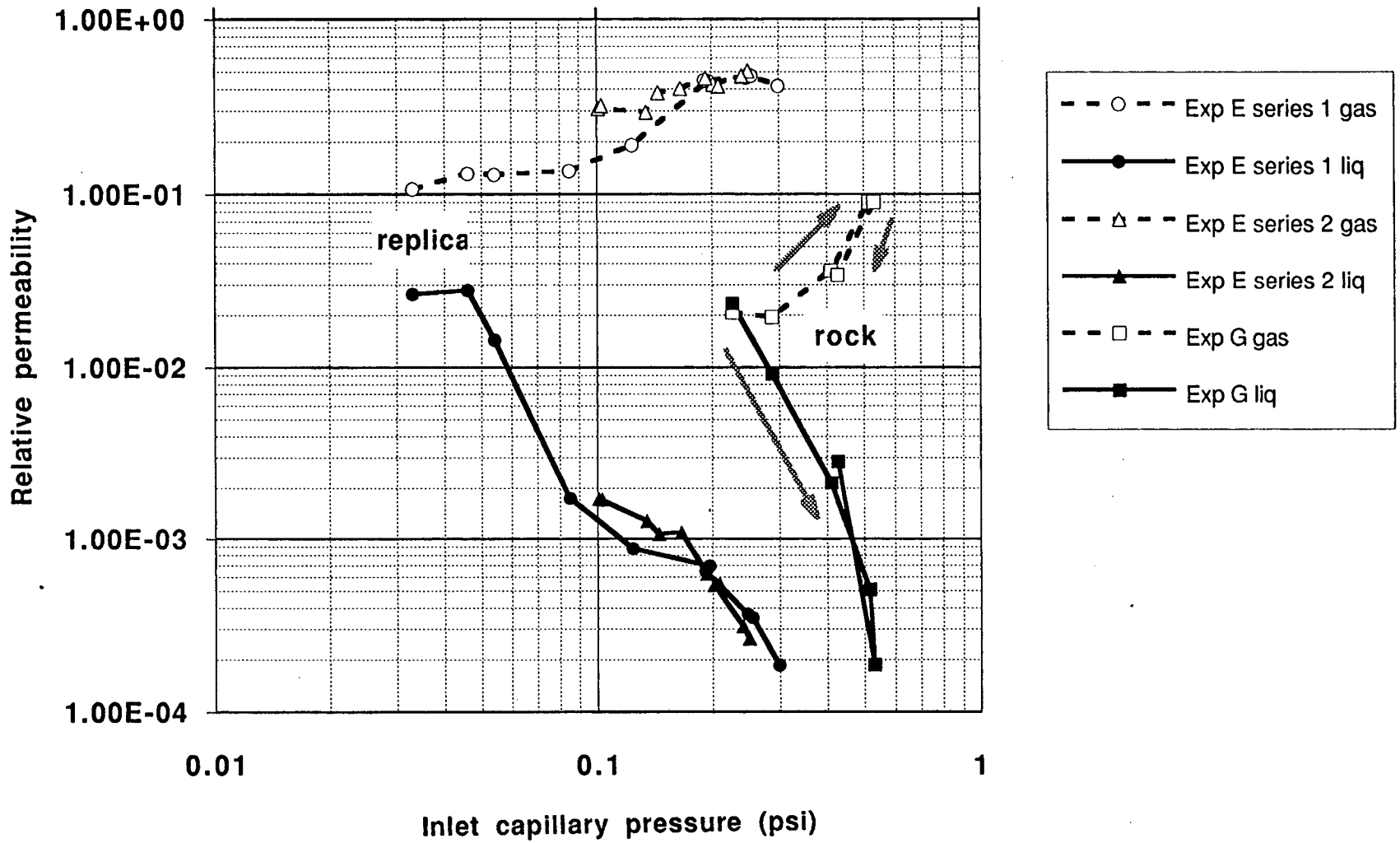
1.00E+00
1.00E-01
1.00E-02
1.00E-03
1.00E-04
Relative permeability
0.01
0.1
1
Inlet capillary pressure (psi)
replica
rock
Exp E series 1 gas
Exp E series 1 liq
Exp E series 2 gas
Exp E series 2 liq
Exp G gas
Exp G liq

Figure 2.

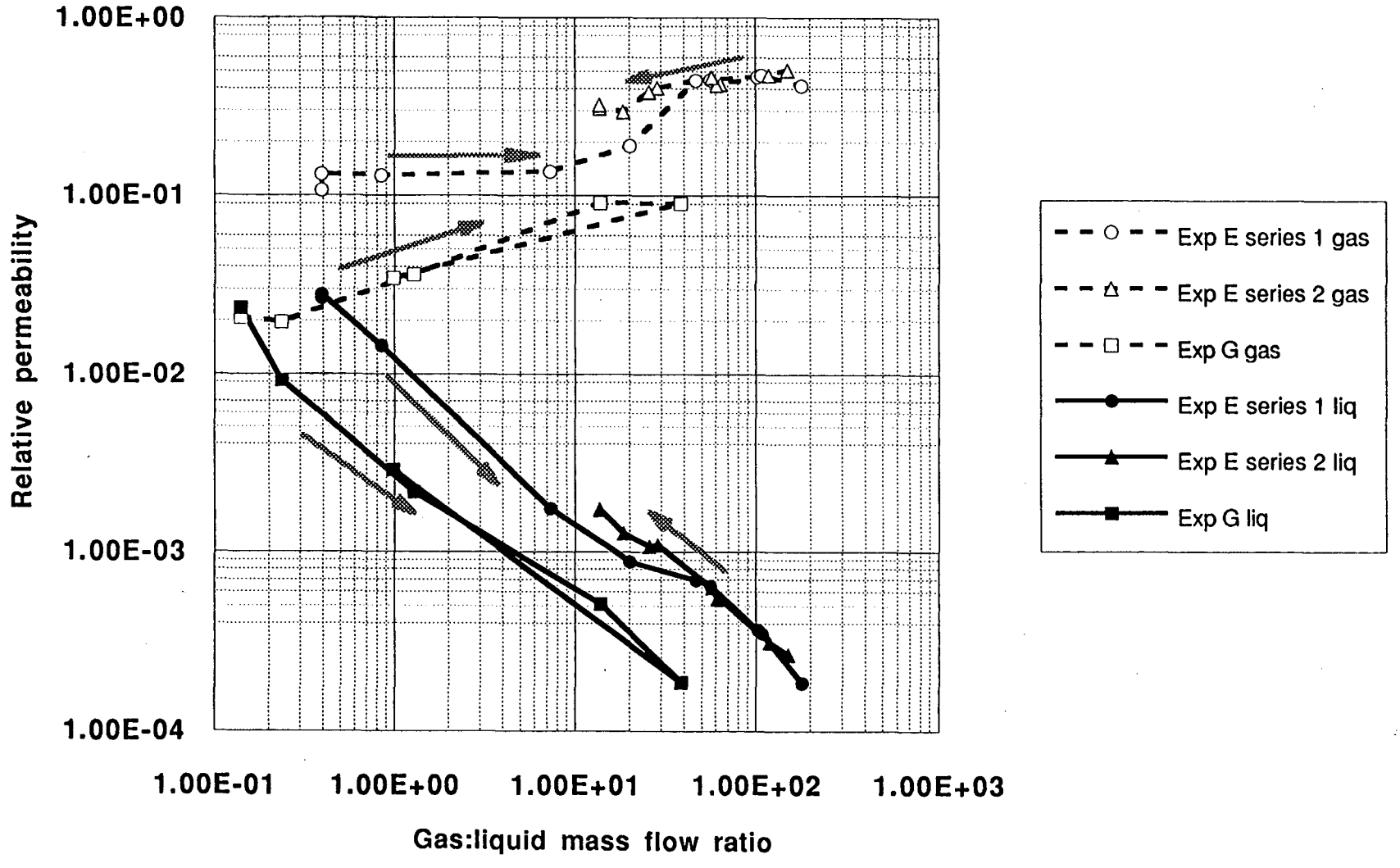
1.00E+00
1.00E-01
1.00E-02
1.00E-03
1.00E-04
Relative permeability
1.00E-01
1.00E+00
1.00E+01
1.00E+02
1.00E+03
Gas:liquid mass flow ratio
Exp E series 1 gas
Exp E series 2 gas
Exp G gas
Exp E series 1 liq
Exp E series 2 liq
Exp G liq

Figure 3.

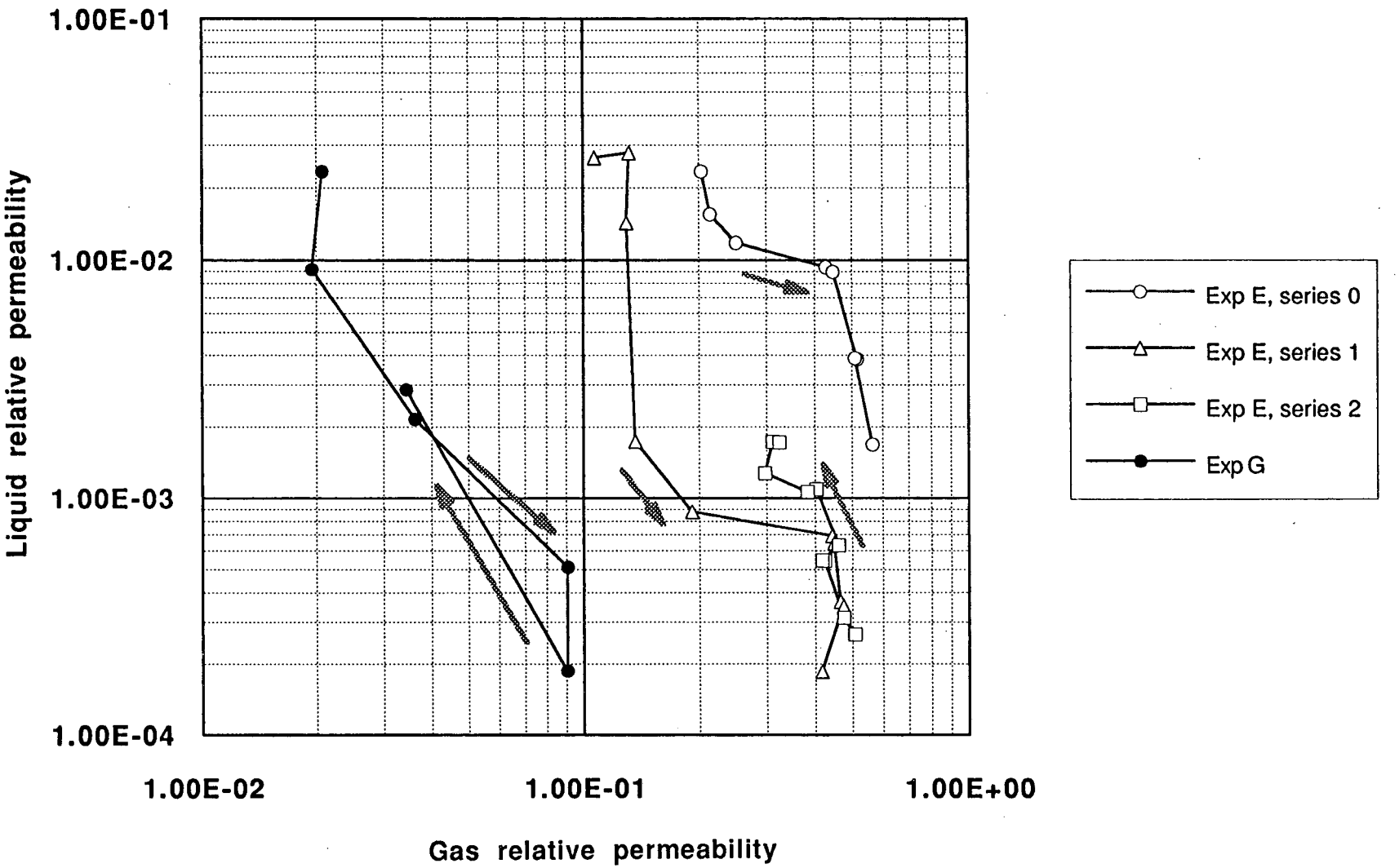
1.00E-01
1.00E-02
1.00E-03
1.00E-04
Liquid relative permeability
1.00E-02
1.00E-01
1.00E+00
Gas relative permeability
Exp E, series 0
Exp E, series 1
Exp E, series 2
Exp G

Figure 4.

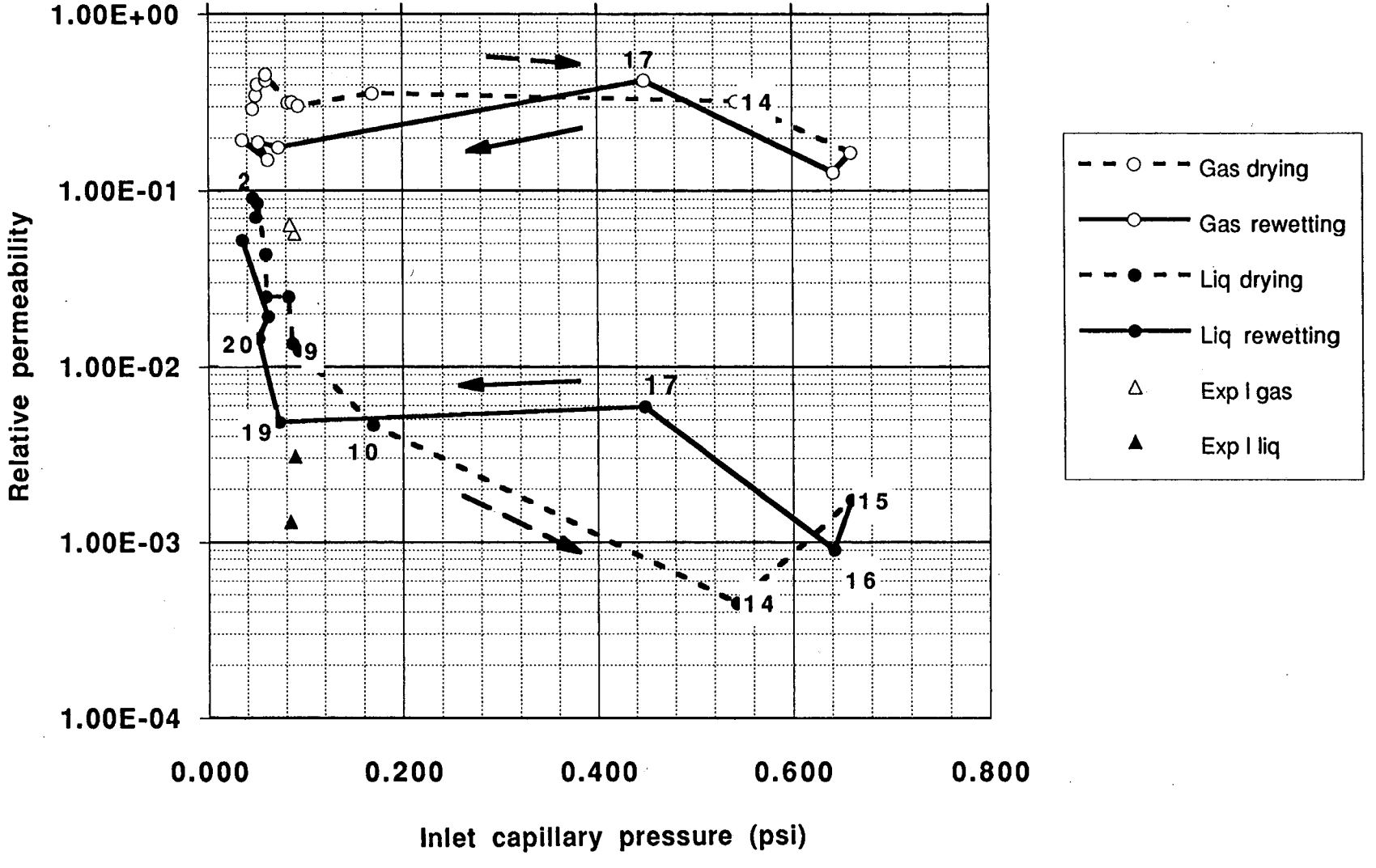
1.00E+00
1.00E-01
1.00E-02
1.00E-03
1.00E-04
Relative permeability
0.000
0.200
0.400
0.600
0.800
Inlet capillary pressure (psi)
17
14
2
20
9
19
10
17
15
16
14
Gas drying
Gas rewetting
Liq drying
Liq rewetting
Exp l gas
Exp l liq

Figure 5.

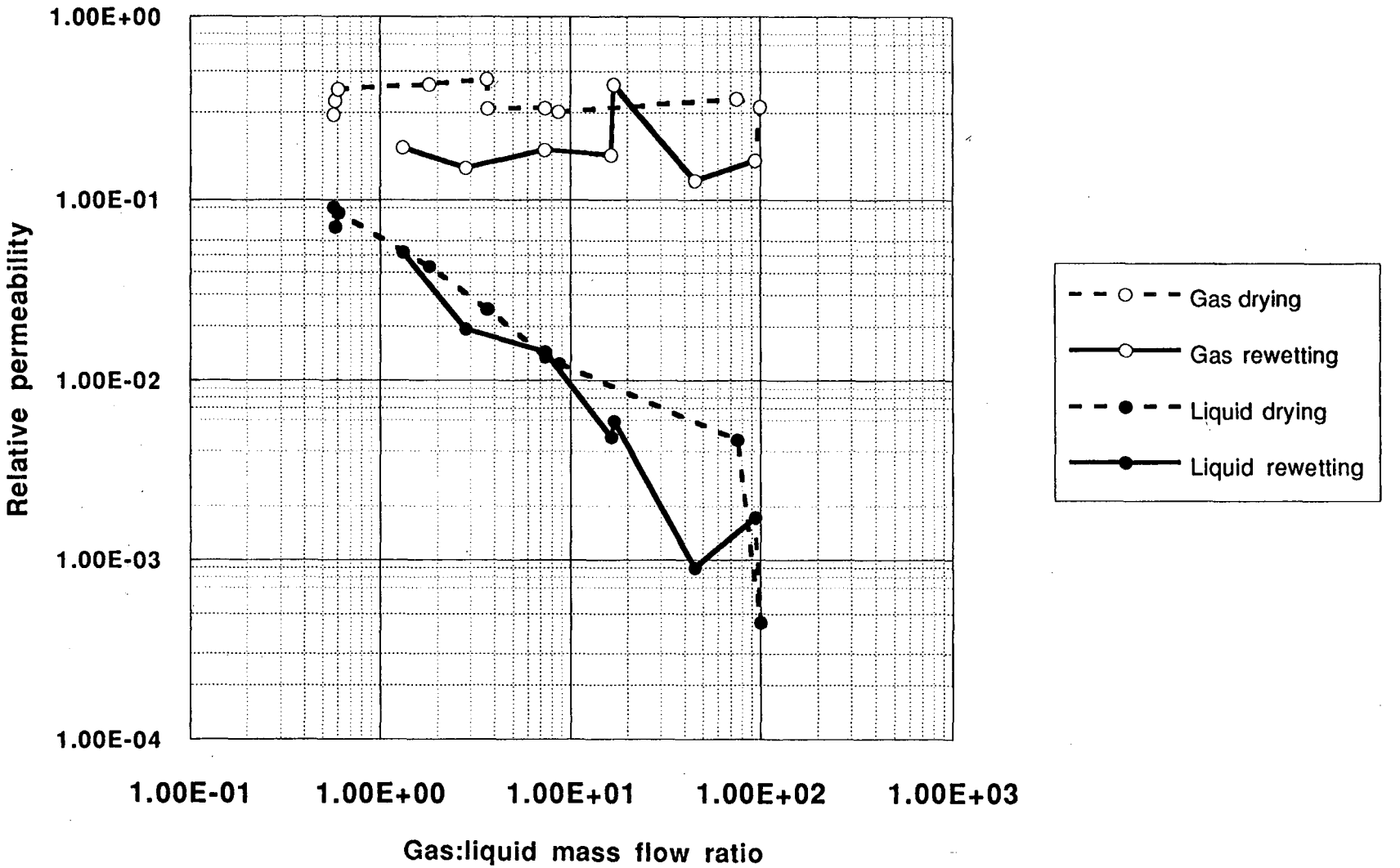
1.00E+00
1.00E-01
1.00E-02
1.00E-03
1.00E-04
Relative permeability
1.00E-01
1.00E+00
1.00E+01
1.00E+02
1.00E+03
Gas:liquid mass flow ratio
Gas drying
Gas rewetting
Liquid drying
Liquid rewetting

Figure 6.

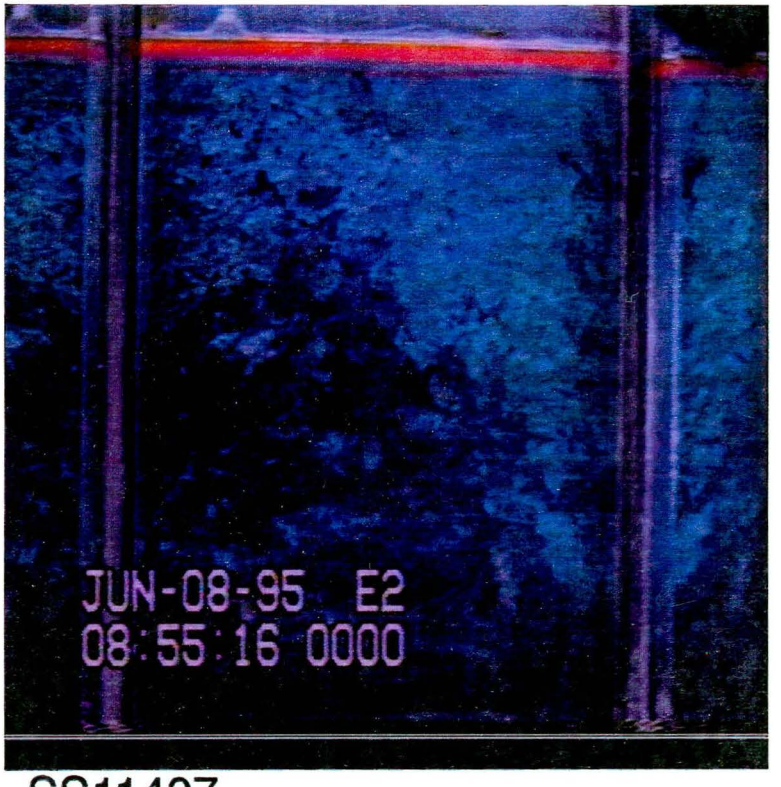

SS11407

XBD 9509-04251

Figure 7.

SS11409

XBD 9509-04254

Figure 8.

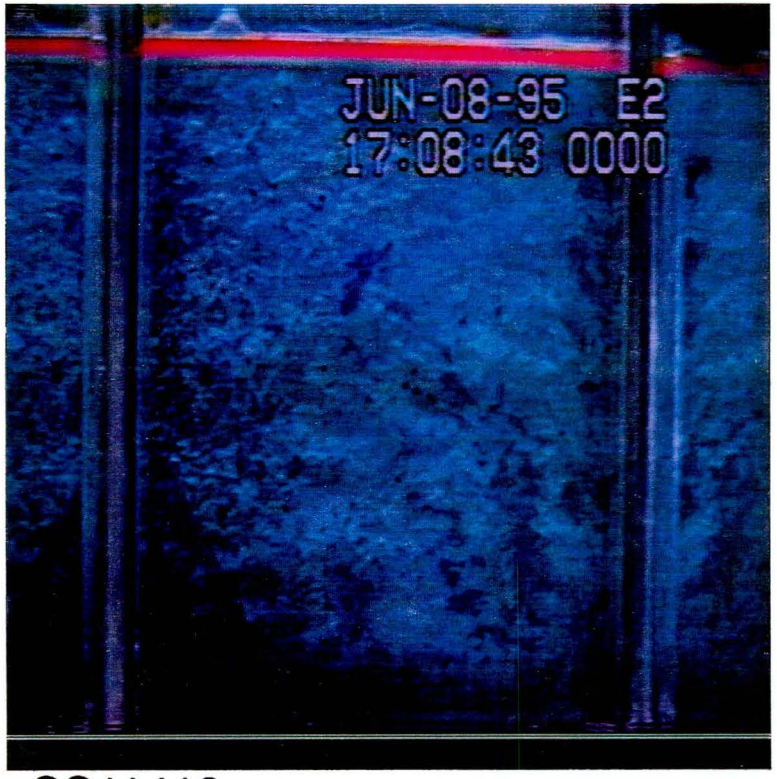

SS11410

XBD 9509-04255

Figure 9.

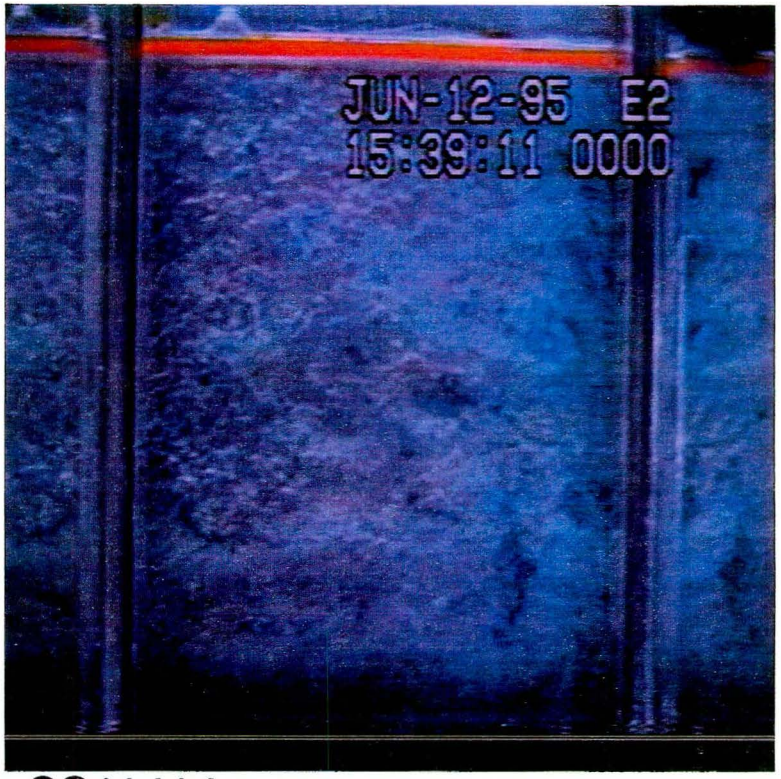

SS11414

XBD 9509-04260

Figure 10.

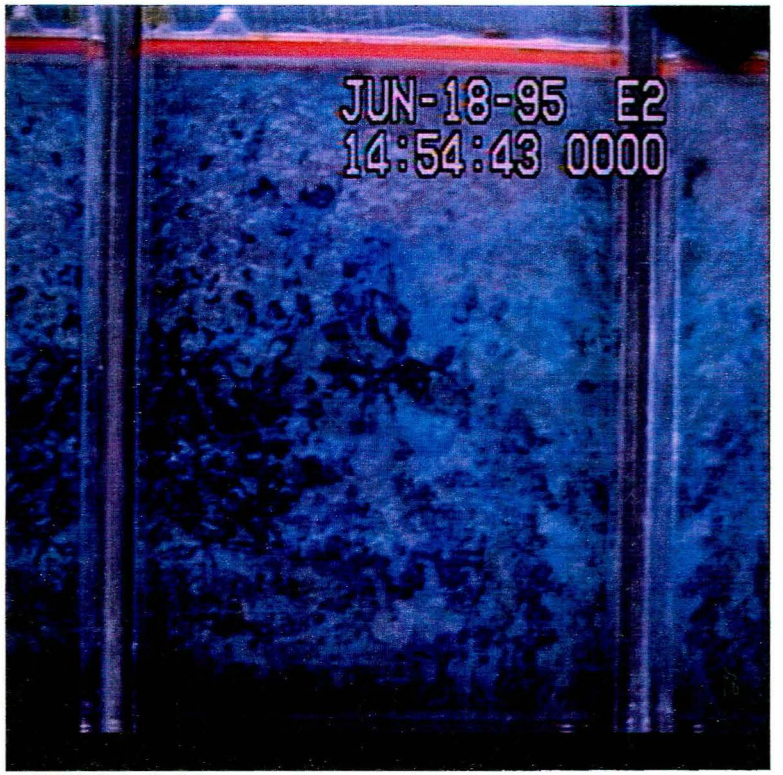

Figure 11.

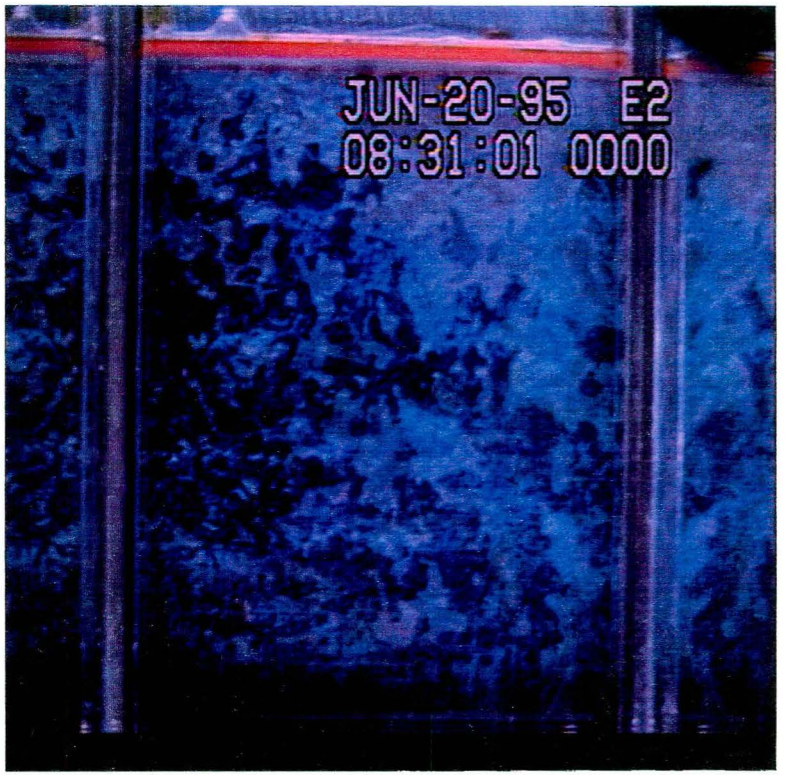

Figure 12.

Figure 13.

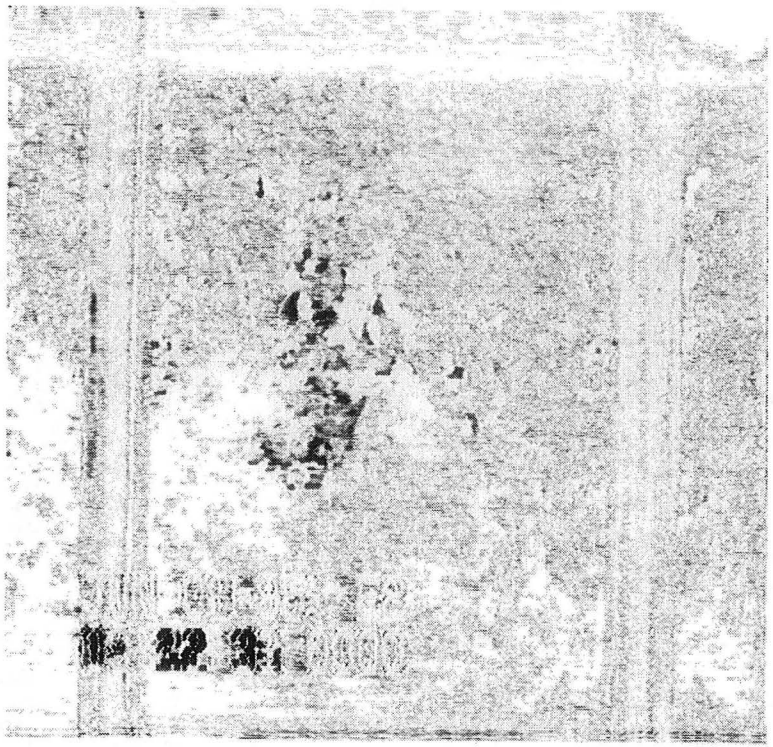

SS11408/11409 DIF

Figure 14.

SS11409/11410 DIF

Figure 15.

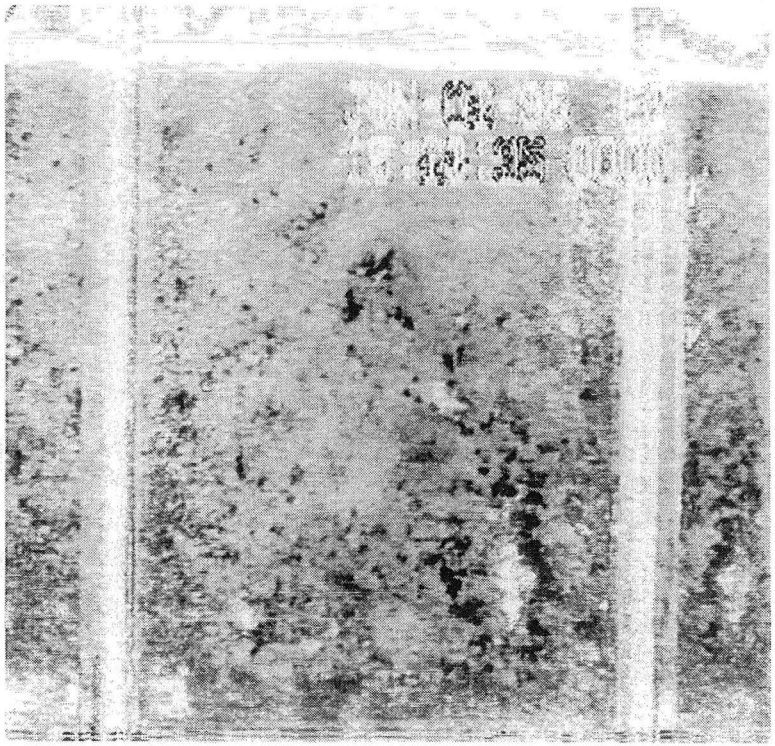

SS11412/11414 DIF

Figure 16.

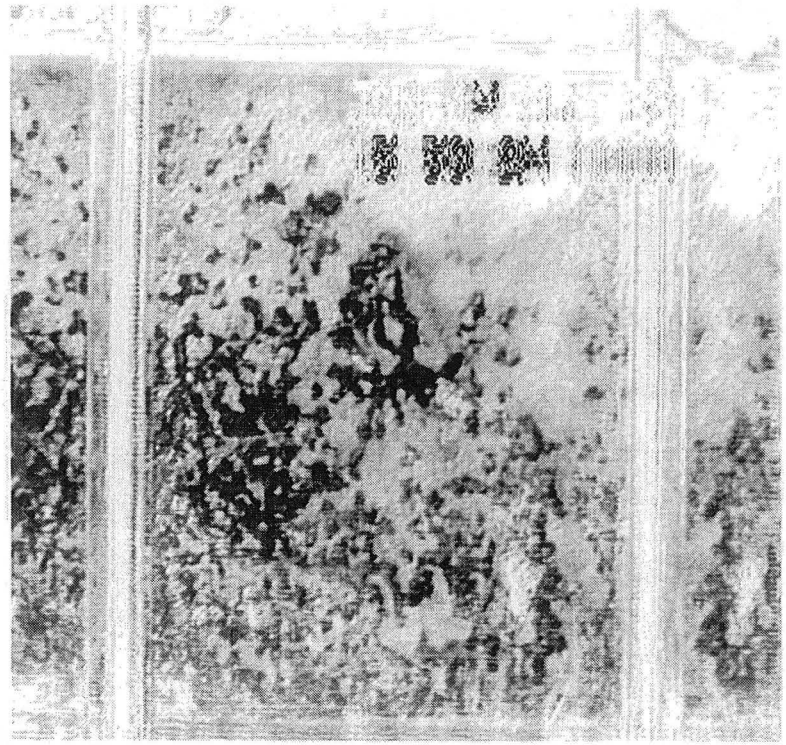

SS11417/11418 DIF

Figure 17.

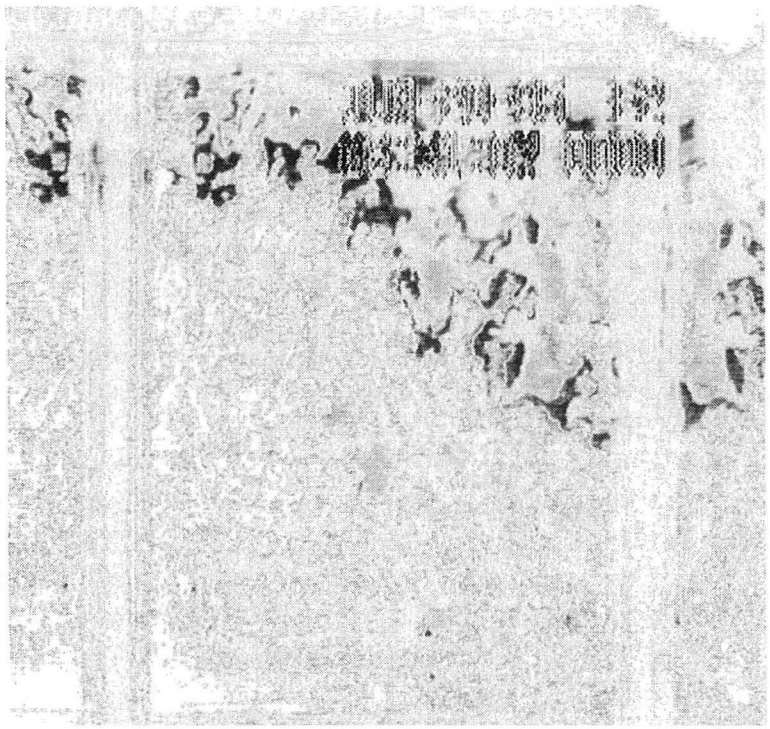

SS11420/11421 DIF

Figure 19.

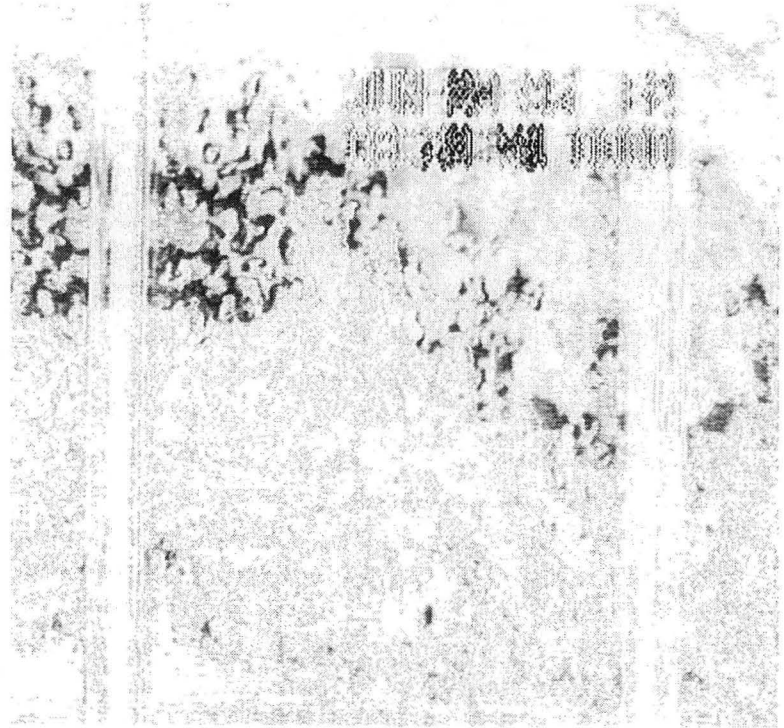

SS11419/11420 DIF

Figure 18.

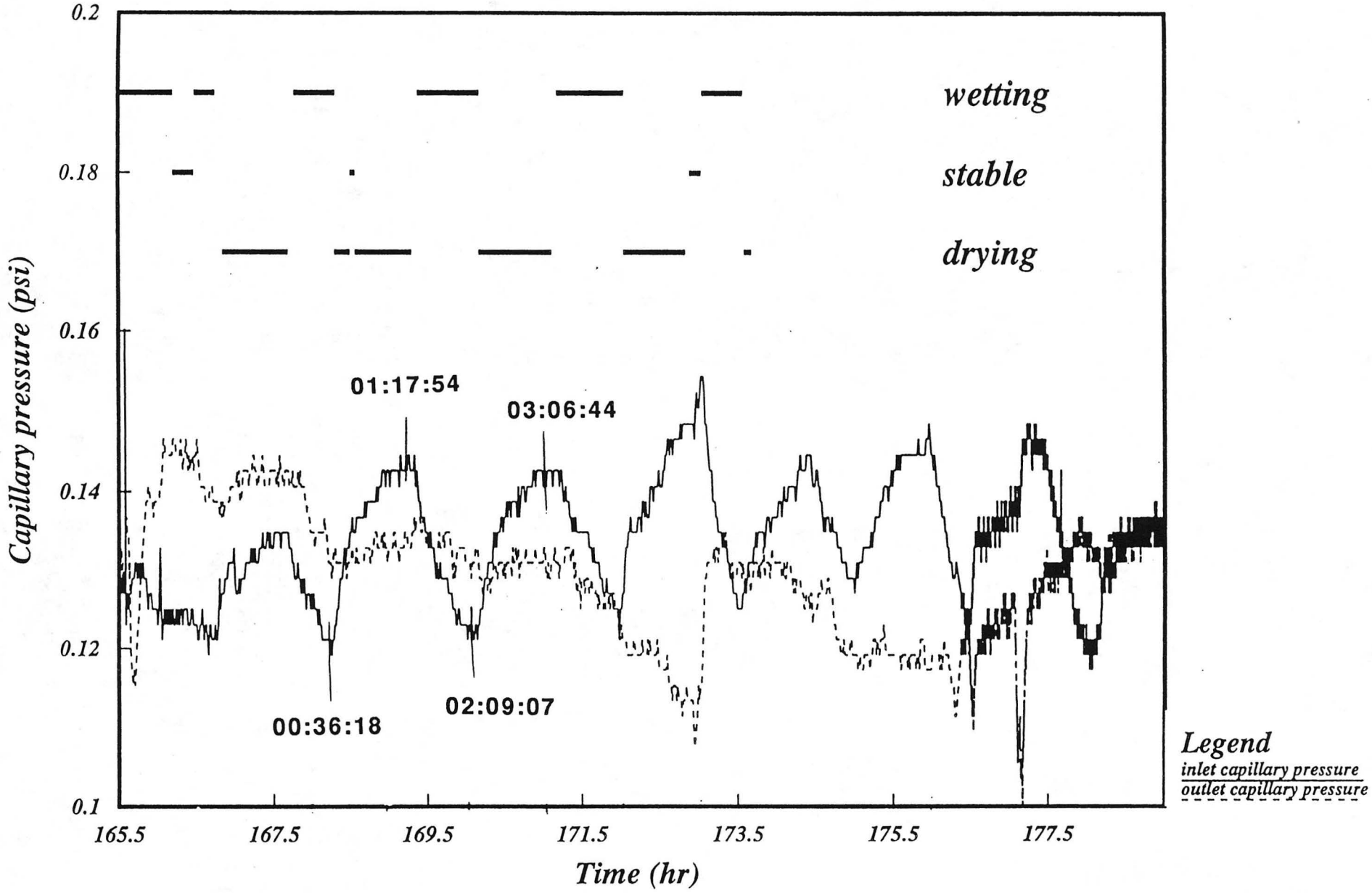
0.2
0.18
0.16
0.14
0.12
0.1
Capillary pressure (psi)
wetting
stable
drying
01:17:54
03:06:44
00:36:18
02:09:07
Legend
inlet capillary pressure
outlet capillary pressure
165.5
167.5
169.5
171.5
173.5
175.5
177.5
Time (hr)

Figure 20.

Appendix A.

Raw Data

These tables summarize the raw data from which all relative permeabilities can be calculated.

Appendix Table G

Exp G condition	Pc in (psi)	Pc in stnd dev	Pc out (psi)	Pc out stnd dev	Pg in (psi)	Pg in stnd dev	Pg out (psi)	Pg out (psi)	Gas flow rate (L/min)	Pl in (psi)	Pl in stnd dev	Pl out (psi)	Pl out stnd dev	dp gas (psi)	dp gas stnd dev	dp liq (psi)	dp liq stnd dev	Liq flow rate (mL/min)
10 1	0.23	0.003	0.207	0.005	15.932	0.023	15.708	0.018	8.00E-04	15.72	0.02	15.5	0.02	0.157	0.005	0.08	0.003	7.50E-03
10 2	0.29	0.003	0.286	0.004	15.913	0.022	15.636	0.018	9.00E-04	15.64	0.02	15.34	0.02	0.189	0.004	0.13	0.003	5.00E-03
10 3	0.41	0.008	0.417	0.025	16.197	0.021	15.783	0.03	3.60E-03	15.88	0.02	15.35	0.01	0.4	0.025	0.41	0.01	3.75E-03
10 4	0.52	0.002	0.517	0.012	16.457	0.02	15.972	0.016	1.04E-02	15.97	0.02	15.45	0.02	0.456	0.008	0.46	0.012	1.25E-03
10 4a	0.53	0.005	0.523	0.005	16.561	0.028	16.073	0.019	1.04E-02	16.07	0.02	15.54	0.02	0.455	0.005	0.46	0.003	6.25E-04
10 5	0.43	0.007	0.406	0.013	16.397	0.024	15.94	0.025	3.72E-03	16.06	0.02	15.52	0.02	0.431	0.008	0.41	0.009	5.00E-03
10 6	0.44	0.002	0.435	0.009	16.309	0.021	15.916	0.02	4.54E-03	15.92	0.02	15.47	0.02	0.367	0.011	0.36	0.001	3.75E-03
10 7	0.5	0.002	0.508	0.004	16.449	0.024	16.007	0.015	6.74E-03	16	0.02	15.49	0.02	0.407	0.006	0.43	0.005	1.25E-03
10 8	0.42	0.002	0.425	0.01	16.291	0.02	15.925	0.018	4.83E-03	15.95	0.02	15.49	0.01	0.339	0.011	0.34	0.004	1.25E-03
10 9	0.41	0.008	0.417	0.043	16.195	0.023	15.917	0.052	3.62E-03	15.86	0.02	15.49	0.02	0.257	0.052	0.27	0.008	6.25E-04
10 10	0.4	0.01	0.395	0.051	16.015	0.044	15.746	0.07	3.79E-03	15.68	0.04	15.34	0.03	0.256	0.063	0.25	0.021	6.25E-04
10 11	0.4	0.006	0.328	0.069	15.936	0.026	15.652	0.069	3.09E-03	15.58	0.02	15.32	0.02	0.273	0.072	0.19	0.006	6.25E-04

Appendix Table H

Exp H condition	Pc in (psi)	Pc in stnd dev	Pc out (psi)	Pc out stnd dev	Pg in (psi)	Pg in stnd dev	Pg out (psi)	Pg out stnd dev	Gas flow rate (L/min)		Pl in (psi)	Pl in stnd dev	Pl out (psi)	Pl out stnd dev	dp gas (psi, manometer)	dp liq (psi)	dP liq stnd dev	Liq flow rate (mL/min)
11.4.2	0.046	0.001	0.069	0.001	16.745	0.021	16.676	0.014	0.023		16.587	0.018	16.564	0.015	0.097	0.043	0.001	5.00E-02
11.4.3	0.049	0.002	0.082	0.001	16.748	0.021	16.679	0.015	0.024		16.608	0.018	16.556	0.016	0.083	0.055	0.001	5.00E-02
11.4.4	0.051	0.002	0.086	0.003	16.749	0.022	16.689	0.016	0.025		16.621	0.017	16.564	0.015	0.074	0.046	0.001	5.00E-02
11.4.5	0.060	0.001	0.080	0.002	16.752	0.021	16.693	0.014	0.025		16.622	0.017	16.573	0.016	0.070	0.030	0.000	1.67E-02
11.4.6	0.060	0.001	0.082	0.001	16.764	0.022	16.708	0.016	0.025		16.651	0.017	16.590	0.016	0.066	0.026	0.000	8.33E-03
11.4.7	0.083	0.001	0.096	0.001	16.829	0.021	16.755	0.016	0.025		16.641	0.016	16.619	0.017	0.096	0.026	0.000	8.33E-03
11.4.8	0.087	0.001	0.101	0.001	16.832	0.022	16.760	0.016	0.025		16.634	0.017	16.618	0.016	0.095	0.024	0.000	4.17E-03
11.4.9	0.093	0.001	0.106	0.001	16.836	0.021	16.771	0.015	0.024		16.641	0.017	16.625	0.017	0.094	0.021	0.001	3.33E-03
11.4.10	0.170	0.001	0.159	0.001	16.892	0.022	16.832	0.014	0.026		16.644	0.019	16.637	0.017	0.086	0.075	0.001	4.17E-04
11.4.14	0.543	0.002	0.558	0.002	16.261	0.020	16.212	0.015	0.014		15.662	0.017	15.633	0.015	0.000	0.029	0.001	1.67E-04
11.4.15	0.660	0.001	0.641	0.001	16.965	0.021	16.877	0.013	0.021		16.204	0.018	16.211	0.015	0.148	0.012	0.001	2.67E-04
11.4.16	0.642	0.001	0.647	0.001	16.963	0.022	16.880	0.016	0.016		16.236	0.018	16.208	0.016	0.145	0.036	0.001	4.17E-04
11.4.17	0.449	0.002	0.435	0.002	16.437	0.020	16.363	0.016	0.012		15.889	0.016	15.899	0.016	0.034	0.011	0.002	8.33E-04
11.4.19	0.073	0.001	0.077	0.002	16.915	0.020	16.819	0.016	0.022		16.720	0.018	16.696	0.018	0.152	0.027	0.001	1.67E-03
11.4.20	0.052	0.001	0.047	0.001	16.892	0.022	16.797	0.016	0.020		16.738	0.020	16.705	0.018	0.128	0.018	0.000	3.33E-03
11.4.22	0.062	0.002	0.061	0.002	16.892	0.021	16.804	0.016	0.015		16.815	0.017	16.696	0.017	0.123	0.027	0.001	6.67E-03
11.4.23	0.035	0.002	0.036	0.002	16.932	0.020	16.850	0.015	0.014		16.892	0.017	16.767	0.017	0.088	0.020	0.001	1.33E-02

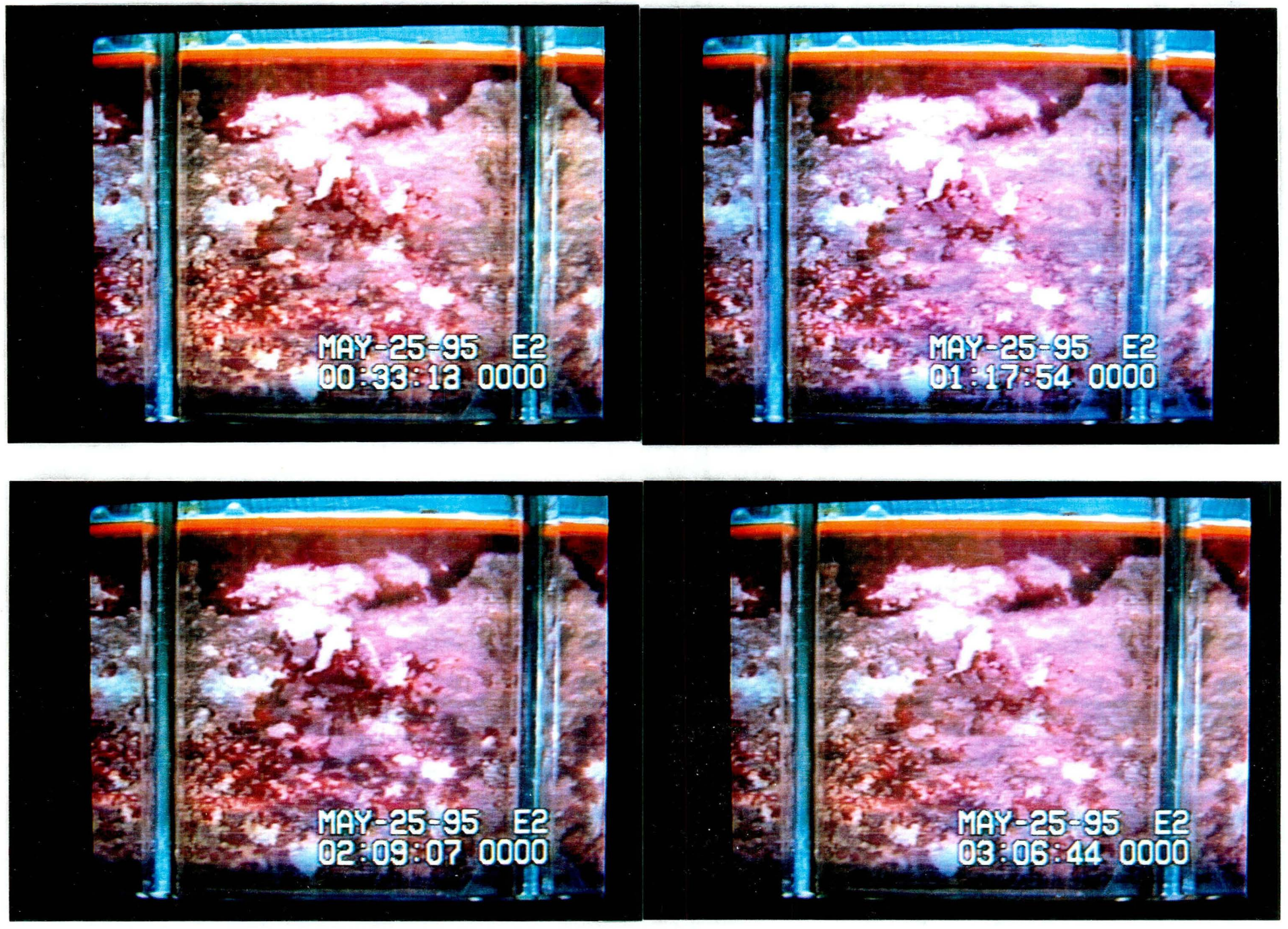
MAY-25-95 E2
00:33:13 0000
MAY-25-95 E2
01:17:54 0000
MAY-25-95 E2
02:09:07 0000
MAY-25-95 E2
03:06:44 0000

Figure 21.

LAWRENCE BERKELEY NATIONAL LABORATORY
UNIVERSITY OF CALIFORNIA
TECHNICAL & ELECTRONIC INFORMATION DEPARTMENT
BERKELEY, CALIFORNIA 94720